Computers and Geotechnics 61 (2014) 67–84

Contents lists available at ScienceDirect

Computers and Geotechnics

journal homepage: www.elsevier.com/locate/compgeo

Finite element analyses of two-tier geosynthetic-reinforced soil walls: Comparison involving centrifuge tests and limit equilibrium results

Suliman B.A. Mohamed [a,1], Kuo-Hsin Yang [a,*], Wen-Yi Hung [b,2]

[a] Department of Civil and Construction Engineering, National Taiwan University of Science and Technology, 43, Sec. 4, Keelung Rd., Taipei 106, Taiwan
[b] National Central University, No. 300, Jhongda Rd., Jhongli City, Taoyuan County 320, Taiwan

ARTICLE INFO

Article history:
Received 15 November 2013
Received in revised form 18 March 2014
Accepted 28 April 2014

Keywords:
Geosynthetic-reinforced soil wall
Multitier wall
Centrifuge test
Limit equilibrium
Finite element
Offset distance
Reinforcement tensile load

ABSTRACT

This study presents the procedure and results of the finite element (FE) analyses of a series of centrifuge tests on geosynthetic-reinforced soil (GRS) two-tier wall models with various offset distances. The objectives of this study were to evaluate the applicability of FE for analyzing GRS two-tier walls with various offset distances and to investigate the performance and behavior of GRS two-tier walls in various stress states. The FE simulations were first verified according to the centrifuge test results by comparing the locations of failure surfaces. The FE results were then used to investigate the effective overburden pressure, mobilization and distribution of reinforcement tensile loads, and horizontal deformation at the wall faces. The interaction between two tiers was investigated based on the FE results, which were also used to examine the modeling assumption of reinforcement tensile loads in limit equilibrium (LE) analysis and to evaluate the design methods in current design guidelines. This study demonstrated favorable agreement between FE and the centrifuge model in locating the failure surface. The FE results indicated that as the offset distance increased, the reinforcement tensile load and wall deformation decreased in both the upper and lower tiers, suggesting the attenuation of interaction between the two tiers. The maximum tensile loads of all reinforcement layers at the wall failure predicted using FE analysis and LE method assuming uniform distribution of reinforced tensile loads were comparable. Compared with the FE results, the Federal Highway Administration (FHWA) design guidelines are conservative in determining the effect of overburden pressure, required tensile strength, location of maximum tension line (for designing the reinforcement length), and the critical offset distance. Furthermore, the FHWA design guidelines do not account for the influence of the lower tier on the upper tier that was observed in this study.

1. Introduction

Geosynthetic-reinforced soil (GRS) walls in a tiered configuration are acceptable alternatives to conventional retaining wall systems because of several benefits such as cost, stability and construction constraints, and aesthetics. In addition, drainage swales or ditches can be installed along the toe of each tier to minimize the surficial flow induced erosion and water infiltration induced instability. The current practice in Taiwan is to apply multitier GRS walls with wrap-around facing, each tier typically being 5 m high, to restore slope and roadway failures induced by heavy rainfall during typhoon seasons. A tiered wall is a transitional structure between a single wall and slope (Fig. 1) that can reduce construction costs and increase system stability compared with a single wall. Because of its configuration, the tiers interact and mutually affect each other. The upper and lower tiers interact through the equivalent surcharge from the upper tier acting on the lower tier, and the vertical and lateral deformation of the lower tier influencing the behavior of the upper tier. Consequently, this interaction can cause additional wall deformation and reinforcement loads in both the upper and lower tiers, compared with a wall of the same height as each tier.

Current design methods [10,5,25] for analyzing GRS multitier walls are based on the lateral earth pressure method, an extension of the design method for analyzing single-tier reinforced walls. The design approaches in these guidelines are considered empirical and are geometrically derived based on the relative distance or offset distance, *D*, between upper and lower tiers. Some studies

* Corresponding author. Tel.: +886 2 2730 1227; fax: +886 2 2737 6606.
E-mail addresses: kobrest@yahoo.com (S.B.A. Mohamed), khy@mail.ntust.edu.tw (K.-H. Yang), wyhung@ncu.edu.tw (W.-Y. Hung).
[1] Tel.: +886 981424577; fax: +886 2 2737 6606.
[2] Tel.: +886 955329820; fax: +886 3 425 2960.

http://dx.doi.org/10.1016/j.compgeo.2014.04.010
0266-352X/

Nomenclature

Basic SI units are given in parentheses

c	cohesion (kPa)
$c_{adjusted}$	adjusted cohesion (kPa)
c_{input}	input cohesion (kPa)
D	offset distance (m)
D_{cr}	critical offset distance (m)
D_{Tmax}	distribution function (dimensionless)
EA	reinforcement stiffness (kN/m)
E_{50}^{ref}	secant modulus (kPa)
E_{oed}^{ref}	tangent modulus for primary oedometer loading (kPa)
E_{ur}^{ref}	unloading–reloading modulus (kPa)
FS	factor of safety (dimensionless)
H	height of two-tiered wall (m)
H_1	height of upper tier (m)
H_2	height of lower tier (m)
K_a	active earth pressure coefficient (dimensionless)
k_r/K_a	normalized lateral earth pressure coefficient (dimensionless)
L_o	reinforcement overlap length (m)
L_1	reinforcement length of upper tier (m)
L_2	reinforcement length of lower tier (m)
m	modulus exponent (dimensionless)
max(T_{max})	maximum reinforcement tensile load (kN/m)
N_g	g-level of centrifuge model (dimensionless)
N_f	failure g-level of centrifuge model (dimensionless)
N_p	input reinforcement tensile strength (kN/m)
q	equivalent uniform load from the upper tier (kN/m^2)
R_f	failure ratio (dimensionless)
S_v	vertical spacing between layers of reinforcement (m)
T_{max}	maximum reinforcement load in each layer (kN/m)
T_{ult}	confined ultimate tensile strength (kN/m)
x	distance from the wall face (m)
y/H	normalized elevation (dimensionless)
z	depth below the surcharge load (m)
z_i	depth to the ith layer of reinforcement (m)
γ	unit weight of backfill soil (kN/m^3)
δ_H	horizontal deformation of wall face (m)
$\delta_{H,max}$	maximum horizontal deformation of wall face (m)
θ	failure plane angle (°)
σ_f	additional vertical stress at the wall face on the ith layer of reinforcement caused by upper tier (kN/m^2)
σ_v	effective overburden pressures (kN/m^2)
σ_z	overburden pressure at depth z (kN/m^2)
v_{ur}	Poisson's ratio for unloading–reloading (dimensionless)
ϕ	peak friction angle (°)
$\phi_{adjusted}$	adjusted peak friction angle (°)
ϕ_{input}	input peak friction angle (°)
ϕ_{ps}	plane strain peak friction angle (°)
ϕ_{tx}	triaxial compression test friction angle (°)
ψ	angle of dilatancy (°)
$\Delta\sigma_v$	additional vertical stress caused by upper tier (kN/m^2)
$\Delta\sigma_{v,i}$	additional vertical stresses from the upper tier acting on the ith layer of reinforcement at the maximum tension line (kN/m^2)
$\Delta\sigma_{v,j}$	additional vertical stresses from the upper tier acting on the jth layer of reinforcement at the maximum tension line (kN/m^2)
ΣM_{sf}	total multiplier defined in PLAXIS (dimensionless)
ΣT_{max}	summation of maximum reinforcement force for all layers (kN/m)

have questioned using this empirical approach [17]. Moreover, the compound wall designs suggested in the design guidelines are complex and require numerous calculation procedures to determine the maximum tension line and additional vertical stress for internal stability analyses. These guidelines do not fully address the interactive mechanism between two tiers and are based only on the additional vertical stresses from the overlying wall tiers acting on the lower tiers. They do not account for the influence of the lower tier on the upper tier.

An alternative to the lateral earth approach is to use the limit equilibrium (LE) method, which is useful for predicting the failure surface location and for assessing the system stability regarding the factor of safety (FS). However, the limitations of LE in analyzing the reinforced structures require assuming the reinforcement tensile load and its inability to predict deformation [18,9]. Although the LE method is applicable to analyzing multitier walls

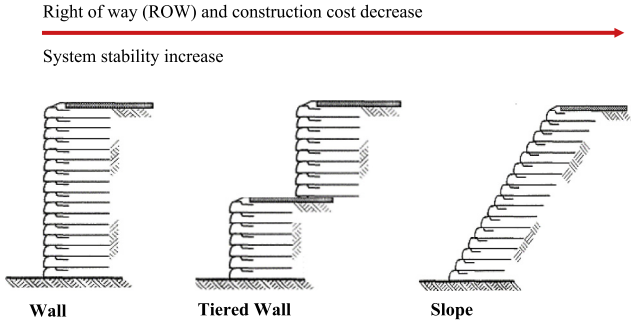

Fig. 1. GRS structures with various configurations.

by comparing its results with those of finite element (FE) analysis [18] and centrifuge tests [24], the modeling assumptions of reinforcement tensile loads require further verification by using the results of measuring physical walls or those of optimally calibrated FE analyses. The FE method has been widely used for modeling reinforced soil structures [35,12,13,15,19,22]. The FE method offers comprehensive information concerning stress, strain, force, and displacement at any location of interest (e.g., at the nodal and Gaussian points). However, the FE method requires comprehensive material characterization and model validation using the measured data from physical walls to produce convincing results. Thus, the FE method combined with experimental test results should be used to investigate the behavior and performance of multitier GRS walls.

Behavior and performance studies of multitier walls are scant, among which multitier walls have been investigated by case studies and field monitoring [20,33,32], full-scale wall tests [37,38], reduced-scale and centrifuge wall tests [36,14], LE analysis [24,17,26,34], and FE analysis [21,36,33,39,38]. Mohamed et al. [24] conducted a thorough review of current design methods and previous studies on multitier walls. Although these studies have addressed crucial issues, most of them have focused on multitier walls with one or two offset distances and lack a comprehensive and consistent comparison of multitier walls with various offset distances. Few studies have quantitatively elaborated on the interactive mechanism discussed at the beginning of this section.

This study conducted a series of FE analyses of twelve GRS two-tier walls with various offset distances and calibrated each FE model according to centrifuge wall models. The objectives of this study were fourfold: (1) to evaluate the FE applicability for analyzing GRS two-tier walls with various offset distances; (2) to

examine the modeling assumption of reinforcement tensile loads in LE analysis and the design methods in current design guidelines; (3) to investigate the performance and behavior of GRS two-tier walls in various stress states; and (4) to investigate the interactive mechanism between two tiers. Based on the FE results, the influence of offset distances on effective overburden pressure, reinforcement tensile loads, wall deformation, and relevant design implications for multitier GRS walls are discussed.

2. Centrifuge tests and limit equilibrium analyses

2.1. Centrifuge tests

Centrifuge modeling has been used for a variety of applications pertaining to geotechnical engineering. Zornberg et al. [41] discussed despite centrifuge modeling has limitations such as the non-uniformity acceleration field, replication of field construction processes and stress paths, boundary effects, and scale effects, the centrifuge provides a useful tool for geotechnical modeling in which prototype structures can be studied as scaled-down models while preserving the stress states required to develop the appropriate soil properties. In this study, a series of centrifuge modeling tests was originally conducted at the National Central University (NCU), Taiwan, to investigate performance and failure mechanisms in two-tier GRS walls. Twelve of these centrifuge model tests were selected for analysis. The details of centrifuge testing program have been reported by Hung [14]. A brief discussion on the wall model and test procedure is given in this section.

For all centrifuge models, the wall heights of the upper and lower tiers were $H_1 = H_2 = 160$ mm, and additional layer of 20 mm of soil was deposited on the top of the upper tier to cover the topmost reinforcement layer. Therefore, the wall models have an equivalent height of 340 mm and were built on a foundation layer 150 mm thick. The corresponding wall heights of prototypes are approximately of 6.5–5.5 m at measured failure g-level of 16–19g. Fig. 2 shows a configuration and schematic profile view of the model wall. Each model was built using the same number of reinforcement layers: 9 for the upper tier and 8 for the lower with 20 mm vertical spacing. Except for the topmost reinforcement, each reinforcement layer were folded back at the face of the wall models, forming a wrap-around facing and a secondary (overlapping) layer (L_o = 40% of reinforcement length for each tier).

Table 1 summarizes the geometrical configuration, reinforcement length and test results (i.e., failure g-level, N_f) for the two-tier GRS wall models with offset distance D ranging from 0 mm to 270 mm. The wall models were grouped into three test series (S, C, and I):

(1) Single (S) series: two wall models were single wall designs with $D \leqslant (H_1 + H_2)/20$ and $L_1 = L_2 = 0.7(H_1 + H_2)$ (i.e., $D \leqslant 16$ mm and $L_1 = L_2 = 224$ mm).
(2) Compound (C) series: eight wall models were compound wall designs with $(H_1 + H_2)/20 < D \leqslant \tan(90° - \phi)H_2$ and $L_1 = L_2 = 0.6\ (H_1 + H_2)$ (i.e., 16 mm $< D \leqslant$ 194 mm and $L_1 = L_2 = 192$ mm). Notably, the selected L_1 is longer than the minimum reinforcement length (i.e., $L_1 = 0.7H_1$) for compound wall design recommended in FHWA design guidelines to prevent the instability of the upper tier during testing.
(3) Independent (I) series: two wall models were independent wall designs with $D > \tan(90° - \phi)H_2$, $L_1 = 0.7H_1$ and $L_2 = 0.7H_2$ (i.e., $D > 194$ mm and $L_1 = L_2 = 112$ mm).

In the first stage, the model wall was supported by a wooden formwork and spun to 40g to compress any voids between the backfill soil and the reinforcement layers through increasing self-weight until the measured settlement at the top of the wall was stable. The centrifuge was then decelerated to a complete stop. In the second stage, the wooden formwork was removed and the models were loaded by gradually increasing their self-weight (by increasing the centrifuge acceleration) in increments of 2g. The weight was maintained for 30 s at each level of acceleration until the model failed. A CCD camera was installed at side of the centrifuge container to record the wall deformation and determine the wall failure.

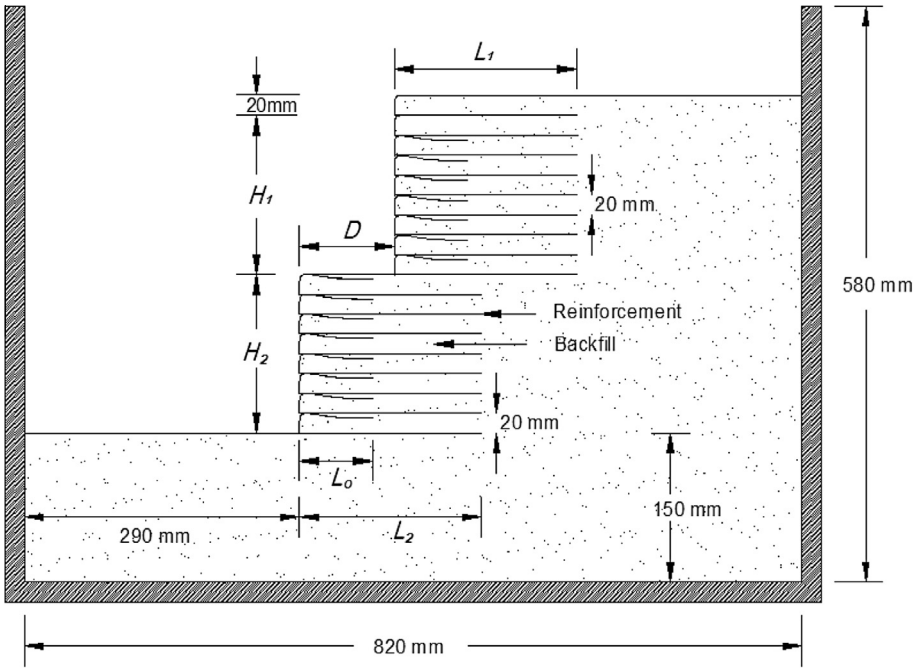

Fig. 2. Configuration and schematic profile view of a centrifuge two-tiered GRS wall model (D is the offset distance; L_1 and L_2 are the reinforcement length of the upper and lower tiers; L_o is the overlap length of reinforcement).

Table 1
Geometrical configurations and test results of two-tiered GRS wall models.

Test no.	Wall parameters		Reinforcement length		Results				
	D	θ	L_1	L_2	N_f	max(T_{max}) (kN/m)		ΣT_{max} (kN/m)	
	(mm)	(deg.)	(mm)	(mm)	(g)	LE	FE	LE	FE
S-series									
1	0	59.0	224	224	16	0.115	0.118	1.96	1.88
2	10	57.8	224	224	18	0.123	0.124	2.09	1.82
C-series									
3	20	56.4	192	192	16	0.105	0.110	1.79	1.51
4	30	55.1	192	192	18	0.112	0.114	1.90	1.62
5	40	53.6	192	192	16	0.092	0.094	1.56	1.40
6	50	52.1	192	192	18	0.098	0.099	1.67	1.35
7	60	50.5	192	192	18	0.092	0.094	1.56	1.43
8	70	48.9	192	192	19	0.092	0.094	1.56	1.46
9	80	47.2	192	192	18	0.077	0.077	1.31	1.18
10	90	45.5	192	192	18	0.069	0.069	1.17	1.01
I-series									
11	260	59.0	112	112	18/17[a]	0.076/0.063[a]	0.075/0.06[a]	0.68/0.50[a]	0.46/0.32[a]
12	270	59.0	112	112	18/18[a]	0.076/0.066[a]	0.072/0.06[a]	0.68/0.53[a]	0.48/0.32[a]

Note: D = Offset distance; θ = Failure plane angle in FHWA design guidelines; L_1 = Reinforcement length of upper tier; L_2 = Reinforcement length of lower tier; N_f = Failure g-level of centrifuge model; max(T_{max}) = Maximum reinforcement tensile force; ΣT_{max} = Sum of maximum reinforcement force for all layers.
[a] Results for upper/lower tier.

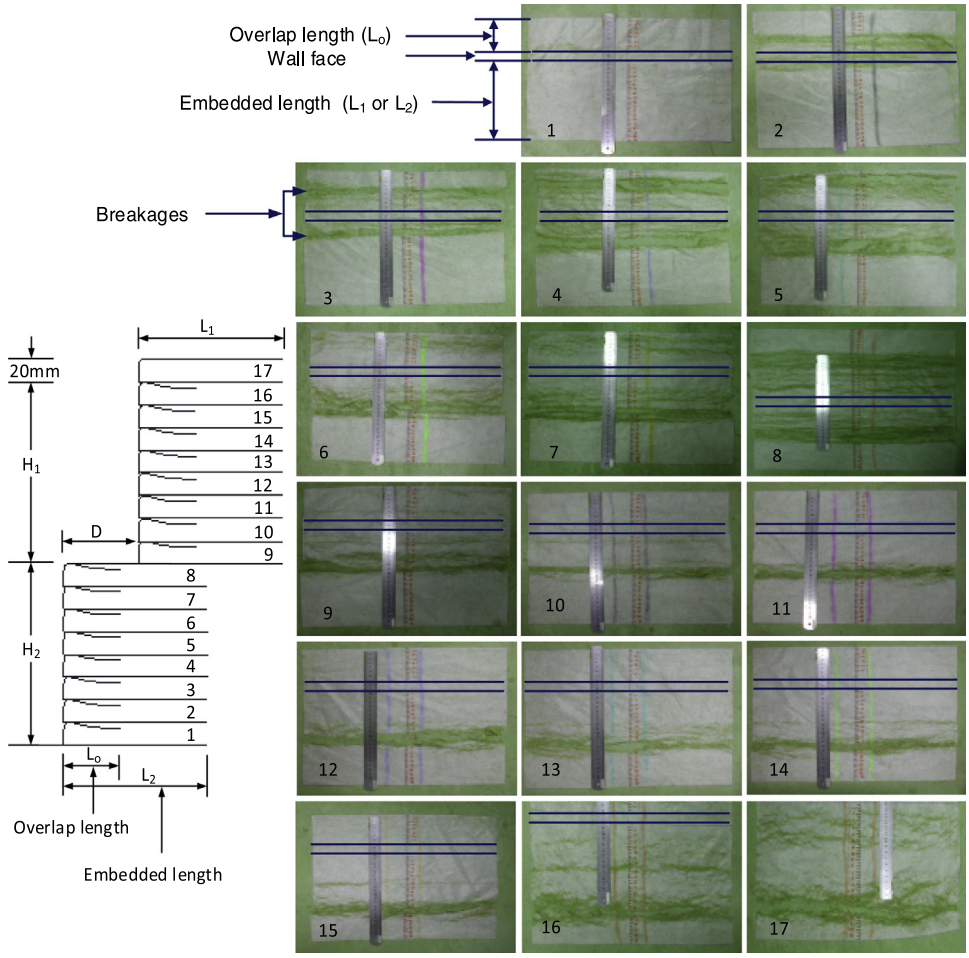

Fig. 3. Breakage pattern in reinforcement material after wall failure in Test C5 (numbers indicate reinforcement level from base to top of wall model).

Fig. 3 shows a broken reinforcement carefully retrieved from the dismantled wall models after tests completed in Test C5. The numbers in Fig. 3 indicate reinforcement level from base to top of wall model. The nearly horizontal breakage pattern in the reinforcement validates the plane strain condition in the centrifuge tests. The reinforcement layers 2–8 show two rupture lines at

Table 2
Properties of the Fulung sand.

Property	Value
Specific gravity, G_s	2.66
Effective size, D_{10} (mm)	0.17
Average size, D_{50} (mm)	0.28
Coefficient of curvature, C_c	1.05
Coefficient of uniformity, C_u	1.78
Maximum dry unit weight, $\gamma_{d,max}$ (kN/m^3)	15.9
Minimum dry unit weight, $\gamma_{d,min}$ (kN/m^3)	13.3
Unit weight, γ (kN/m^3)	15.0
Triaxial compression friction angle, ϕ_{tx} (°)	39.5
Plane strain friction angle, ϕ_{ps} (°)	42.3

opposite sides of wall face (the blue[3] double lines in Fig. 3) indicate the failure surface cutting through both the primary reinforcement and the overlapping length. The location of the critical failure surface was determined based on the observed tears (ruptures) in each layer of the reinforcement.

2.2. Material properties

The soil used in the centrifuge test was clean and uniform Fulung beach sand, classified as poorly graded sand (SP) in the Unified Soil Classification System. Table 2 summarizes the properties of the Fulung sand used as the backfill and foundation material. The backfill unit weight of sand and the friction angle obtained in a series of triaxial compression tests at the target relative density $D_r = 70\%$ were $\gamma = 15$ kN/m^3 and $\phi_{tx} = 39.5°$, respectively. To characterize the shear strength of the test sand under the plane strain condition in the centrifuge model, the plane strain peak friction angle ($\phi_{ps} = 42.3°$) was estimated using the correlation between the triaxial compression friction angle and the plane strain friction angle [16]:

$$\phi_{ps} = 1.5\phi_{tx} - 17 \quad (1)$$

The geotextile used in the centrifuge study was nonwoven polyester, rayon fabric. A series of unconfined wide-width tensile tests [3] and zero-span tests with clamps 6 mm apart [28] were performed to evaluate the strength properties of the geotextile material. The strain ratio of both tensile tests is controlled at 10%/min. The average tensile strength T_{ult} for the geotextile were 0.05 kN/m from wide-width tests and 0.12 kN/m from zero-span test.

2.3. Limit equilibrium analyses

In this study, limit equilibrium analyses were performed to predict the locations of failure surfaces and to assess the maximum mobilized tensile forces of reinforcement in two-tier GRS wall models. The failure surfaces and maximum mobilized tensile forces identified by the LE analyses are compared with those identified by centrifuge tests and finite element simulations as discussed further below. The LE calculations were performed using Spencer's method [31] to search for noncircular failure surfaces as coded in the Slide v.6.0 program [29]. The shear strength of the test sand in the centrifuge model was characterized by the plane strain friction angle ($\phi_{ps} = 42.3°$). The geotextile was modeled as a reinforcement element by inputting a tensile strength value and a coverage ratio of 100%. Centrifugal force was simulated by increasing the unit weight of backfill N_f times corresponding the target g-level at failure.

[3] For interpretation of color in Figs. 3 and 7, the reader is referred to the web version of this article.

The limit equilibrium analyses assumed a uniform distribution of reinforcement tensile forces with depth, horizontal orientation of reinforcement forces, and considered overlapping geotextile length as an additional reinforcement layer that increased stability in the wall. The input tensile strength of reinforcement was varied iteratively while holding all other soil variables constant until computed factor of safety (FS) of wall system equal to 1.0. The calculated values are summarized in Table 1. This estimate accounted for the maximum mobilized tensile force (or confined ultimate tensile strength T_{ult} of reinforcement) which was expected to equal the average in-soil reinforcement tension at the moment of failure. Additional details for the search for the noncircular critical surface and validation of modeling assumptions of reinforcement load in the LE analysis are provided by Mohamed et al. [24].

3. Finite element analyses

A commercial FE program, PLAXIS v. 8.2 [27], was used for the FE analyses on the centrifuge models in this study. The FE simulations were first verified according to the centrifuge test results by comparing the failure surface locations. The FE results were then used to investigate the performance and behavior of two-tier walls with various offset distances and to examine the modeling assumption of reinforcement tensile loads in LE analysis and the design methods in the current design guidelines. The details of FE modeling are presented in subsequent sections.

3.1. Finite element model and calculation procedure

Fig. 4 shows the photo and FE mesh for centrifuge Model C5 under initial conditions. A 15-node triangular element with 12 stress points under plane strain conditions was designated for the soil element. The mesh coarseness was set as "fine," which generated approximately 1226 triangular elements for a given geometry. Reinforcement was simulated using a 5-node geogrid element with five stress points. Both primary and overlapping reinforcement layers were considered in the FE model as indicated in Fig. 4. Standard boundaries were imposed to simulate confinement at the edges of the aluminum centrifuge box. Layer-by-layer stage construction and the centrifuge test procedure described in Section 2.1 were simulated numerically.

The centrifugal forces within test models were simulated by increasing the soil unit weight N_g times on each soil element. At each loading stage, the simulation increased the centrifugal load by 2g until the measured failure g-level was reached. The tolerated error value of 1% was set as the global convergence criteria (i.e., unbalanced force divided by current external force). As suggested in the PLAXIS manual, the tolerated error value was increased to 3%, which was associated with the arc-length function at the final loading stage to avoid the numerical convergence problem at the verge of structure failure.

After the simulated g-level reached the measured failure g-level, a *phi*/*c* reduction function was activated to determine the wall system safety factor. In the *phi*/*c* reduction analysis, the strength parameters $\tan\phi$ and c of the soil are successively adjusted until the GRS wall approaches the verge of failure. The FS is computed as follows:

$$\mathrm{FS} = \sum M_{sf} = \frac{\tan\phi_{input}}{\tan\phi_{adjusted}} = \frac{c_{input}}{c_{adjusted}} \quad (2)$$

where ΣM_{sf} is the total multiplier defined in PLAXIS [27]. The value of ΣM_{sf} is equivalent to the value of FS; ϕ_{input} and c_{input} are the original input soil strength properties (i.e., plane strain soil shear strength in this study), and $\phi_{adjusted}$ and $c_{adjusted}$ are the adjusted soil strength properties calculated during the *phi*/*c* reduction analysis.

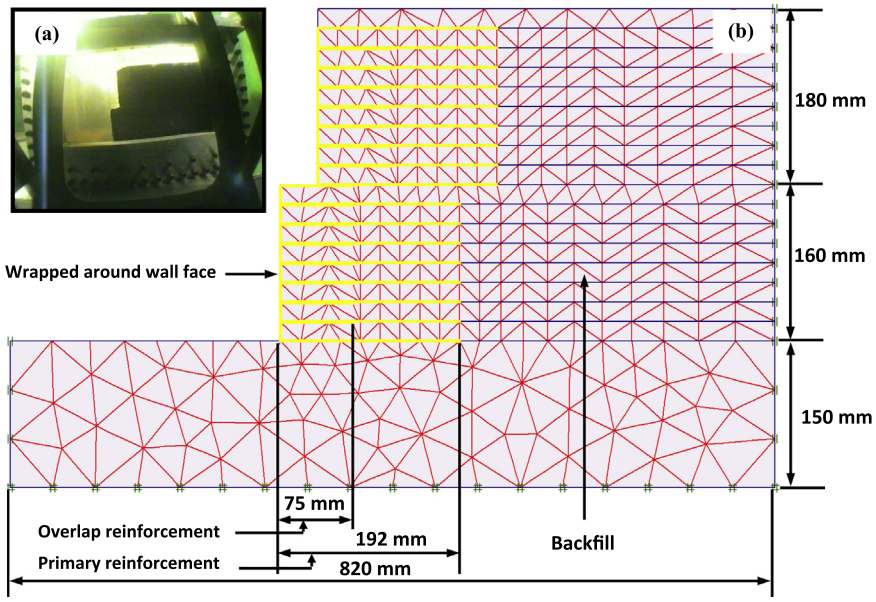

Fig. 4. Configuration of model in Test C5: (a) centrifuge at initial condition; (b) finite element setup and initial mesh.

3.2. Backfill soil modeling

Backfill Fulung sand was modeled as a stress-dependent, hyperbolic elasto-plastic material using the Hardening Soil model [30]. Table 3 lists the soil properties of Fulung sand calibrated using triaxial compression tests. The backfill dilation angle (ψ) was estimated based on the empirical relationship $\psi = \phi - 30^{o}$ proposed by Bolton [6]. A low cohesion value ($c = 2$ kPa) was introduced in the soil model to prevent premature soil yielding in a local low-confining pressure zone. Fig. 5 shows the measured and predicted results of the stress–strain-volumetric response of Fulung sand for $D_r = 70\%$ under triaxial compression tests. Fig. 5 shows that the Hardening Soil model accurately captures the stress–strain relations until the peak shear strength of the soil is reached, but is incapable of modeling the strain-softening behavior in the post-peak region.

To account for plane strain conditions in the centrifuge tests, the soil properties under plane strain conditions were used for FE simulations in this study. Because of lacking test data of Fulung sand under plane strain conditions, the plane strain soil properties were deduced from the soil properties calibrated from triaxial compression tests. The plane strain peak friction angle ($\phi_{ps} = 42.3°$) was estimated using Eq. (1). Regarding the soil modulus, Marachi et al. [23] reported that for the same minor principal stress value, the initial plane-strain response was stiffer than the response for the same material under triaxial test conditions. Hatami and Bathurst [12] inspected the data from triaxial compression and plane strain tests and reported that the elastic modulus ratio of Royal Military College sand from the plane strain test results to triaxial compression test results is approximately 2.25. In the current study, the plane strain secant modulus was estimated using the E_{50}^{ref} obtained from the triaxial test times the ratio of the peak shear strength under plane strain conditions to that under triaxial compression conditions (i.e., $\tan\phi_{ps}/\tan\phi_{tx}$). This approach simply assumes the failure strains in triaxial tests and the plane strain are similar. Consequently, the secant modulus

Table 3
Backfill soil properties used in finite element model.

Property	Boundary conditions	
	Axisymmetric (triaxial)	Plane strain[a]
Stiffness properties (Hardening Soil model)		
E_{50}^{ref}, secant modulus (kPa)	48,000	52,800[c]
E_{oed}^{ref}, tangent modulus for primary oedometer loading (kPa)	47,000	47,000
E_{ur}^{ref}, unloading–reloading modulus (kPa)	144,000 [d]	158,400[d]
m, modulus exponent	0.5	0.5
R_f, failure ratio	0.9	0.9
ν_{ur}, Poisson's ratio for unloading–reloading	0.2	0.2
Strength properties		
ϕ, peak friction angle (°)	39.5	42.3[b]
c, cohesion (kPa)	2	2
ψ, angle of dilatancy (°)	10	12
Bulk unit weight of backfill		
γ, unit weight (kN/m^3)	–	15

[a] Plane strain values were used in FE model for sand backfill.
[b] Estimated by $\phi_{ps} = 1.5\phi_{tx} - 17$ suggested by Lade and Lee [16].
[c] Assumed to be $\tan\phi_{ps}/\tan\phi_{tx} \times E_{50}^{ref}$.
[d] Assumed to be 3 E_{50}^{ref} as the default value in PLAXIS.

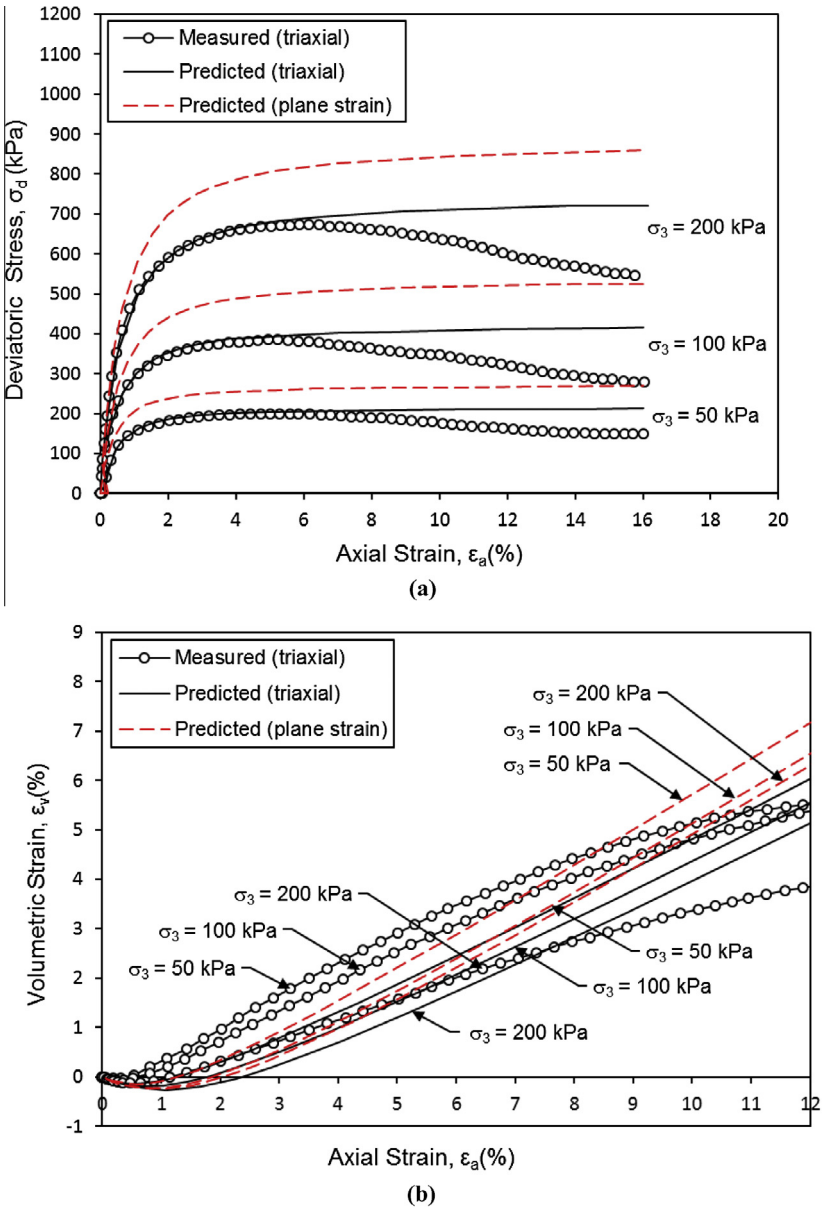

Fig. 5. Comparison of predicted and measured stress–strain-volumetric response of Fulung sand under triaxial compression tests and plane strain conditions: (a) stress–strain; (b) volumetric strain–axial strain.

increased by a factor of 1.1 to simulate the plane strain condition, as indicated in Table 3. Fig. 5 shows the predicted results of the stress–strain-volumetric response of Fulung sand for $D_r = 70\%$ under plane strain conditions.

3.3. Reinforcement modeling

The nonwoven geotextile reinforcement was modeled as a linear elastic–perfect plastic material with an axial stiffness, but without bending stiffness. In addition, the geogrid element can sustain tensile force, but not compression. As the nonwoven geotextile tensile behavior was found to be affected by soil confinement and geotextile impregnation by soil particles [7]. Therefore, when simulating reinforcement behavior within centrifuge models, the confined load–strain response should be used to model the nonwoven geotextile. However, experimentally quantifying in-soil tensile properties (i.e., tensile strength and stiffness) of the low strength nonwoven geotextile is difficult. Moreover, the in-soil tensile properties for each centrifuge test are likely subjected to change because of various magnitudes of soil confinement acting on reinforcement induced by different *g*-levels and offset distances of wall models. The likely range for in-soil tensile property value of the nonwoven geotextile can be defined using the wide-width test (for reinforcement under no or low confinement) and the zero-span tensile test (for reinforcement under high confinement) [8,42]).

Similar to the approach adopted in LE analysis, the input tensile strength of reinforcement, N_p, was systematically varied until the FS = 1.0 ± 1% calculated by *phi*/*c* reduction. Table 1 presents a summary of the final input values of reinforcement tensile strength. This approach warranted the limit state condition in the FE analysis to subsequently identify a relevant failure mode. For simplicity, the reinforcement stiffness was input as $EA = 0.66$ kN/m (Fig. 6), corresponding to the secant stiffness at 50% ultimate tensile strength of reinforcement by using the load–strain response obtained from the zero-span tensile test. A sensitivity study of FE

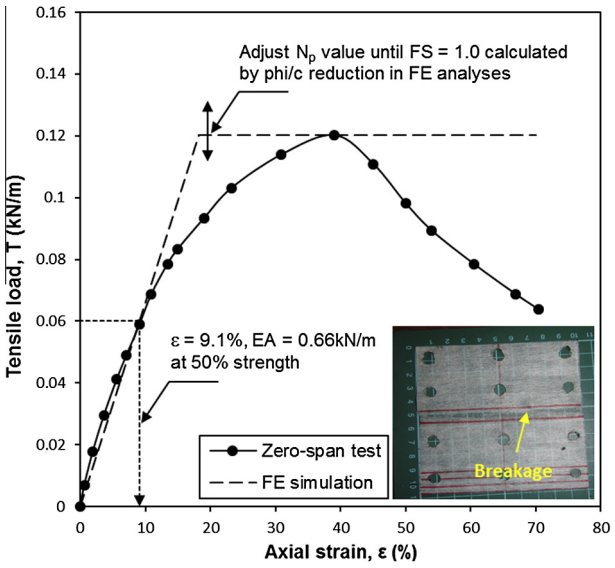

Fig. 6. Predicted and measured load–strain responses of nonwoven geotextile.

models with and without soil-reinforcement interface elements was conducted to evaluate the effect of considering pullout failure mechanism on the predicted results. An 80% of soil peak shear strength, a typical value for soil–geotextile interaction, was assumed for the interface shear strength in this sensitivity study. The numerical results indicated that the effect of considering pullout failure mechanism on the FE results (the T_{max} distribution with depth and location of failure surface) is insignificant. Finally, the soil-reinforcement interface was modeled as fully bounded in this study. This approach was also supported by visual inspection after the centrifuge models collapsed. As shown in Fig. 3, the primary failure mode of the centrifuge models resulted from reinforcement breakage rather than pullout.

4. Model verification

4.1. Comparison of failure surface location

The FE model was verified by comparing the measured locations of failure surfaces obtained from centrifuge tests with the predicted results from the FE analyses. Fig. 7 shows the comparison results of Tests S1, C4, C6, and I11. The failure surface of the centrifuge wall model (black triangles in Fig. 7) was identified by tears (ruptures) in each reinforcement layer (Fig. 3). The failure surface in the FE analysis (color contour in Fig. 7) was determined by the contour of the most intense incremental shear strain. As can be seen in Fig. 7, the FE and centrifuge models show good agreement in the failure surface location, demonstrating the capability of FE modeling to predict the observed failure patterns for two-tier walls with various offset distances.

Fig. 8 shows the mobilized tensile load distribution along the reinforcement layers in Test C4 by increasing the *g*-level. The failure surface location obtained from the centrifuge test and LE agree with the locus of the maximum reinforcement tensile load at each reinforcement layer obtained by FE. This agreement is consistent with the field observations of a full-scale, instrumented, and reinforced soil slope in Zornberg [40] and the FE analysis of two centrifuge reinforced soil slopes in Yang et al. [35], showing that the maximum strain in each reinforcement layer corresponds to the trace of potential failure surface in the slope.

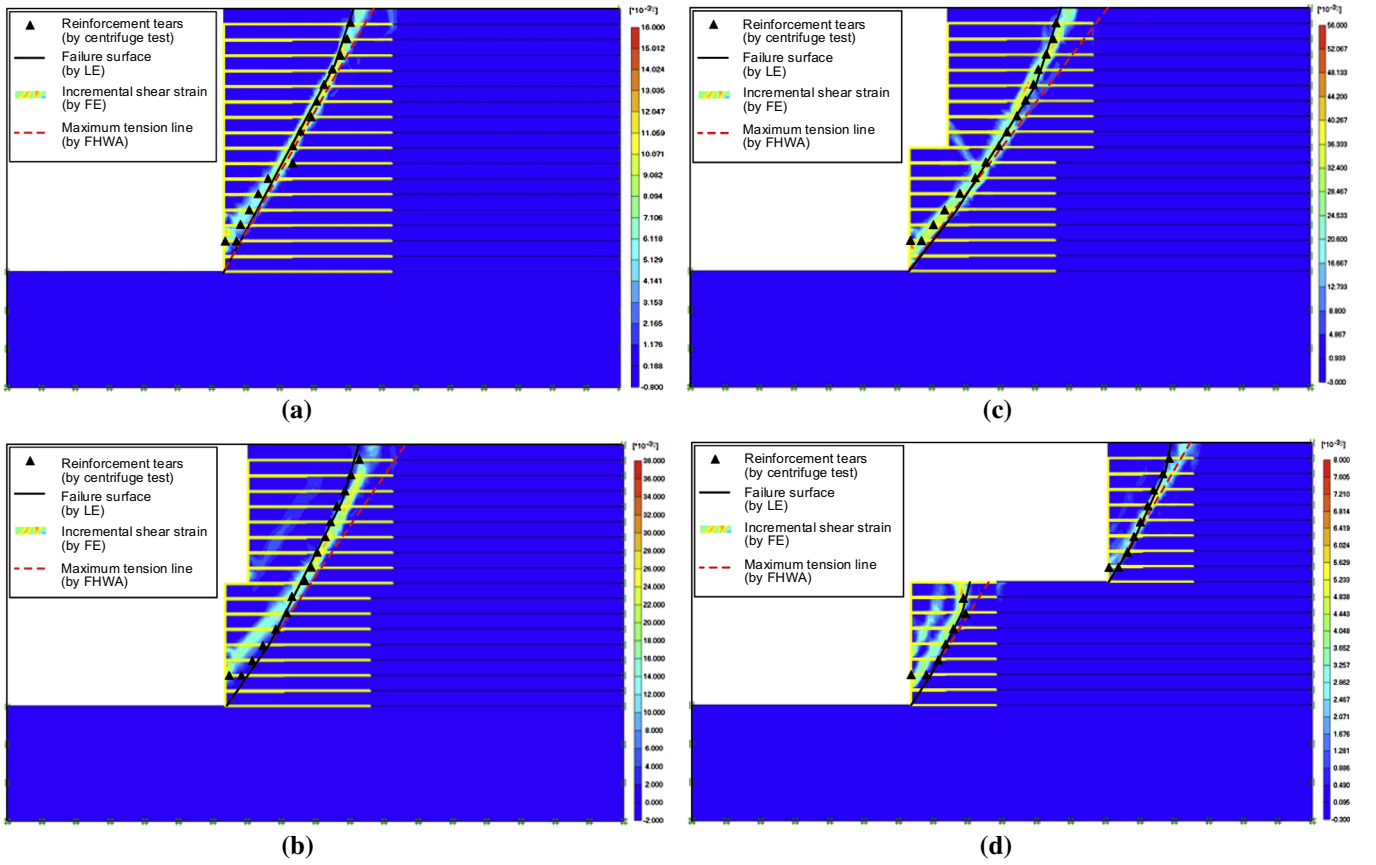

Fig. 7. Predicted and measured locations of failure surfaces from centrifuge tests: (a) Test S1; (b) Test C4; (c) Test C6; (d) Test I11.

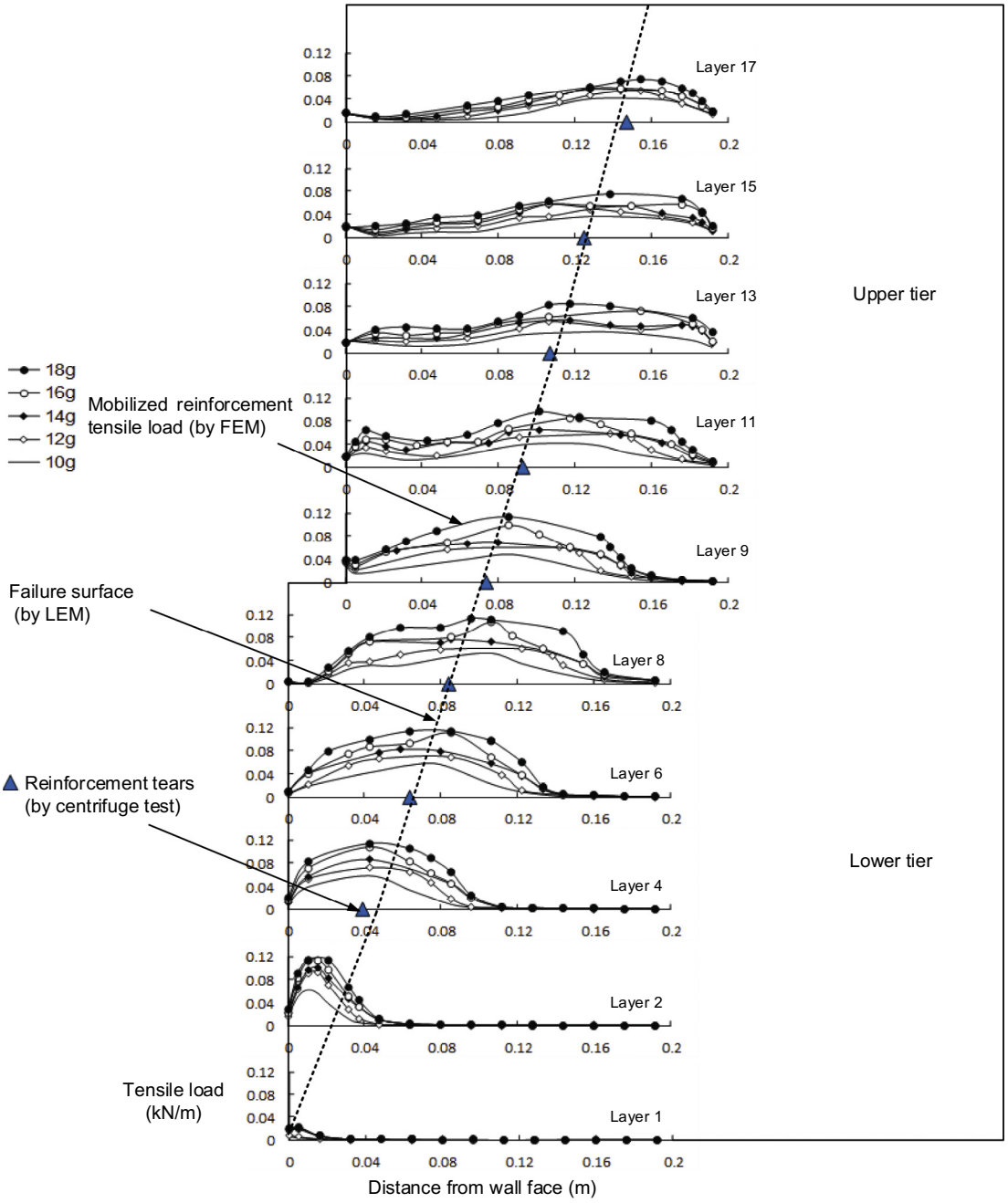

Fig. 8. Mobilized tensile load distributions along reinforcement layers in Test C4 predicted from FE analyses.

The failure surfaces predicted by FE analysis in most centrifuge models (Fig. 7) passed through the lower tier at the second reinforcement layer rather than at the wall toe. This observation is consistent with the centrifuge test results (e.g., no evidence of breakages in the retrieved reinforcement at the lowermost layer) in previous studies by Zornberg et al. [41] and Yang et al. [35]. Allen et al. [2] addressed the similar attenuating effects of stiff competent foundations on reinforcement loads at the wall base. The boundary constraint from the dense and shallow foundation in centrifuge models likely prevented failure surfaces from passing through the wall toe. This firm foundation constrained soil movement and reinforcement deformation at the wall base. Therefore, strains that develop in the bottommost reinforcement layer are too low to cause failure, as shown in Fig. 8, in which the tensile loads that developed at the first reinforcement layer are nearly negligible at all *g*-levels.

This section also presents the results of examining the failure surface locations predicted by LE analyses and maximum reinforcement tension lines, an indicator of failure surface, as suggested by FHWA design guidelines. The failure surface in LE analysis (solid line in Fig. 7) was defined by searching for the noncircular critical failure surface. Because the failure surface in the LE analysis passed through the wall toe, the predicted failure surface at the lower tier slightly differs from those identified in FE analyses and centrifuge tests, but agrees at the upper tier. Fig. 7 also shows maximum tension lines (dash line) suggested by FHWA design guidelines. The comparison results showed that the predicted maximum tension lines agree satisfactorily with experimental failure surfaces in single and independent wall models. However, the maximum tension lines depict the failure surfaces at a long distance from the wall face in compound wall models, particularly for the upper part of the upper tier. Therefore, using maximum

tension lines recommended by FHWA design guidelines in compound wall designs results in overestimating the required reinforcement lengths against pullout.

4.2. Comparison of mobilized maximum tensile load

Although the predicted values of the maximum tensile loads from all layers, max(T_{max}), calculated in the FE analyses (Table 1) indirectly verify the FE model, they possess a rational physical meaning. The calculated max(T_{max}) values were bounded between the unconfined T_{ult} values obtained by the wide-width and zero-span tests. This numerical result was supported by other studies [8,42]) which have demonstrated that the likely range for the in-soil tensile strength value of the nonwoven geotextile can be defined using wide-width and zero-span tensile tests. Table 1 shows that the calculated max(T_{max}) values decreased with an increased offset distance, suggesting that an increased offset distance decreases the influence of the equivalent surcharge from the upper tier on reinforcements in the lower tier, which subsequently decreases the max(T_{max}). The highest max(T_{max}) value was acquired from single walls because of their small offset distances, which induced a high overburden pressure on the reinforcement. Independent walls had the lowest confined max(T_{max}) values because the large offset distance decreased the overburden pressure from the upper tier acting on reinforcements in the lower tier.

5. Results and discussion

The results of FE analysis on the centrifuge models were used to investigate the mobilization and distribution of reinforcement tensile loads, effective overburden pressure, and the deformation of wall faces of two-tier walls with various offset distances. The FE results were also used to examine the modeling assumption of reinforcement tensile loads in LE analysis and the design methods in the current design guidelines. The resulting insights into GRS multitier wall design are discussed.

5.1. Effective overburden pressure

The effective overburden pressure σ_v on the lower tier wall was evaluated by comparing the FE results with those calculated using the FHWA design guideline approach ([5,10]), and the modified Gray's elastic solution [34]. The σ_v is defined as:

$$\sigma_v = \Delta\sigma_v + \sigma_z \tag{3}$$

where σ_v is the effective overburden pressure acting on the reinforcement, $\Delta\sigma_v$ is the additional vertical stress from the upper tier acting on a reinforcement layer in the lower tier, and σ_z is the overburden pressure from the top of the lower tier. Estimating the effective overburden pressure accurately is critical because the σ_v value is directly applied to evaluate the reinforcement tensile load and pullout resistance in the internal stability analyses against reinforcement breakage and pullout.

In the FHWA approach, the additional vertical stress $\Delta\sigma_v$ (due to the influence of the equivalent surcharge from the upper tier) relies on D and H_1. Three cases are suggested in the FHWA design guidelines to calculate $\Delta\sigma_v$. In Case I, the case with a small offset distance, $D \leqslant \tan(45^\circ - \phi/2)H_2$, the additional vertical stress is calculated as the equivalent uniform surcharge from the upper tier (i.e., $\Delta\sigma_v = \gamma H_1$). In Case III, the case with a large offset distance, $D > \tan(90^\circ - \phi)H_2$, two tiers are not considered superimposed (i.e., $\Delta\sigma_v = 0$) when assuming that no interaction exists between the two tiers and they are designed as two independent walls. For the case with an intermediate offset distance between these limits, $\tan(45^\circ - \phi/2)H_2 < D \leqslant \tan(90^\circ - \phi)H_2$, denoted as Case II in the FHWA design guidelines, the additional vertical stress can be evaluated using the following equations and illustrated in Fig. 9.

$$\Delta\sigma_{v,i} = \frac{\gamma H_1 - \sigma_f}{(z_2 - z_i)\tan(45^\circ - \phi/2)}x + \sigma_f \tag{4}$$

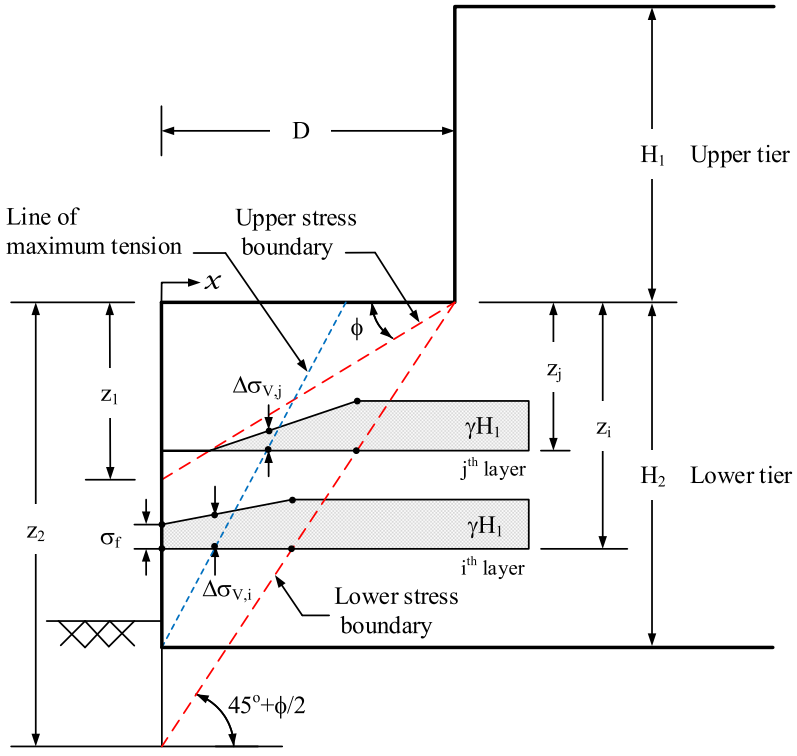

Fig. 9. Illustration of additional vertical stress calculated in the Case II in the FHWA design guidelines (modified from [10,5]).

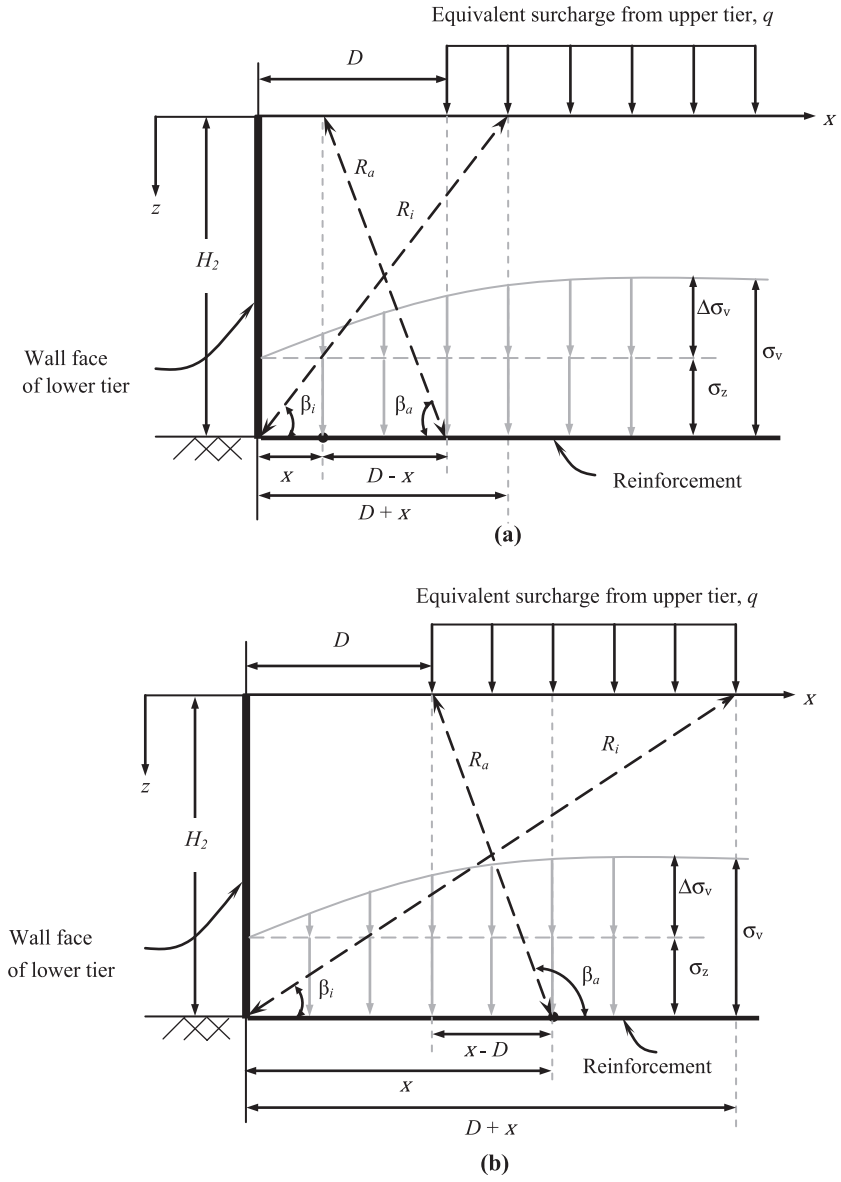

Fig. 10. Illustration of additional vertical stress calculated by the modified Gray's elastic solution for a flexible multi-tiered wall: (a) $x < D$; (b) $x \geqslant D$ (modified from [34].

$$\Delta\sigma_{v,j} = \frac{\gamma H_1 [z_1 x - D(z_1 - z_j)]}{z_1 (z_2 - z_j) \tan(45^\circ - \phi/2) - D(z_1 - z_j)} \tag{5}$$

$$\sigma_f = \frac{z_i - z_1}{z_2 - z_1} (\gamma H_1) \tag{6}$$

$$z_1 = D \tan(\phi) \tag{7}$$

$$z_2 = D \tan\left(45^\circ + \frac{\phi}{2}\right) \tag{8}$$

where $\Delta\sigma_{v,i}$ and $\Delta\sigma_{v,j}$ are the additional vertical stresses from the upper tier acting on the ith and jth reinforcement layers at the maximum tension line, σ_f is the additional vertical stress from the upper tier acting on the ith reinforcement layer at the wall face, z_i and z_j are the depths of the ith and jth reinforcement layers, z_1 and z_2 are the depths of the upper and lower stress boundaries at the wall face, and x is the distance behind the lower tier wall face. The FHWA design guidelines empirically assume $\Delta\sigma_v = 0$ for the area to the left of the upper stress boundary and $\Delta\sigma_v = \gamma H_1$ for the area to the right of the lower stress boundary. Inside the two stress boundaries, $\Delta\sigma_{v,i}$ and $\Delta\sigma_{v,j}$ are interpolated linearly in the horizontal direction between σ_f and γH_1 for the ith layer and between 0 and γH_1 for the jth layer, respectively.

Based on Gray's elastic method [11], Wright [34] proposed a modified elastic solution for estimating $\Delta\sigma_v$ of a "flexible" multi-tier wall due to the effect of overlying wall tiers. The $\Delta\sigma_v$ on a reinforcement layer at a given location (x, z) is defined by the following equations:

$$\Delta\sigma_v = \frac{q}{\pi}\left[\left(\beta_a + \frac{(x - D)z}{R_a^2}\right) - \left(\beta_i + \frac{(-x - D)z}{R_i^2}\right)\right] \tag{9}$$

where q is the equivalent uniform surcharge from the upper tier, x is the horizontal distance from the wall face, D is the offset distance, z is the depth below the top of the lower wall, and β_a, β_i, R_a, and R_i are indicated in Fig. 10 and formulated as follows:

$$\beta_i = \tan^{-1}\left(\frac{z}{D + x}\right) \tag{10}$$

$$\beta_a = \tan^{-1}\left(\frac{z}{D - x}\right) \quad \text{for } x < D \tag{11a}$$

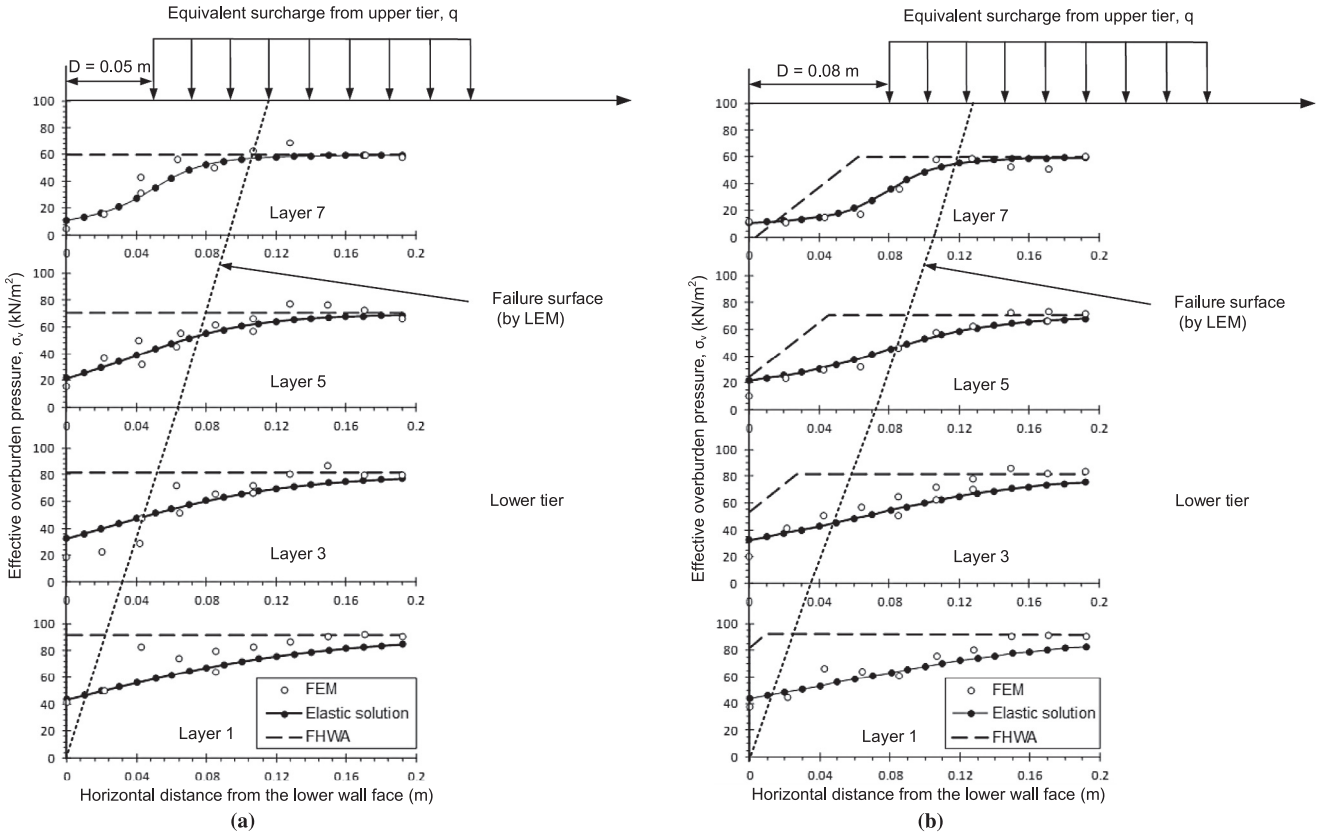

Fig. 11. Calculated σ_v distribution along reinforcement layers using FE, modified Gray's elastic solution, and FHWA approach: (a) Test C6; (b) Test C9.

$$\beta_a = \pi + \tan^{-1}\left(\frac{z}{D-x}\right) \quad \text{for } x \geqslant D \tag{11b}$$

$$R_i = \sqrt{z^2 + (D+x)^2} \tag{12}$$

$$R_a = \sqrt{z^2 + (D-x)^2} \tag{13}$$

Fig. 11 shows the comparison results of the σ_v distribution along the first (bottom), third, fifth, and seventh reinforcement layers in the lower tier wall calculated using the FE method, the modified Gray's solution, and the FHWA approach. The results in Fig. 11 show that the modified Gray's method agrees satisfactorily with the FE results for estimating the σ_v distribution along the reinforcement layers. The FHWA approach predicts substantially high vertical stresses compared with those predicted using the FE and the modified Gray's methods, resulting in an overestimate of the tensile load and pullout resistance of reinforcement for internal stability analyses. The modified Gray's method is an alternative method that produces preferable results for calculating $\Delta\sigma_v$.

5.2. Reinforcement tensile load

Fig. 12 shows the development and distribution of the maximum tensile loads with depth for various g-levels obtained by FE analysis in Tests S1, C4, C6, and I11. The results in Fig. 12 indicate that maximum tensile loads linearly increase in depth for various loading increments. The reinforcement reaches its ultimate tensile strength, as shown in a uniform distribution, at the lower part of the wall at wall failure. The reinforcement strain data from instrumented full-scale walls support these numerical results. Stuedlein et al. [32] reported that the measured reinforcement loads increased in depth below the top of a 46-m high, four-tier MSE wall. Yoo and Jung [37] investigated the long-term performance and behavior of 5.6 m high, two-tier GRS walls. The measured strains on various reinforcement layers presented in Fig. 15 in Yoo and Jung [37] infer increased tensile force with depth. The linear load distributions with depth observed for the numerical results under working stress conditions in this study and in two wall cases previously discussed differ from the trapezoidal distribution obtained for several well instrumented, full-scale, single GRS walls [1,2,4].

For internal stability against reinforcement breakage, an accurate evaluation of reinforcement loads is critical. This study used the reinforcement tensile load information obtained from FE analyses to examine the modeling assumption of reinforcement tensile loads in LE analysis and the design methods in the current design guidelines, discussed as follows. In the LE analysis, because of the problem of statically indeterminate when incorporating reinforcements into analysis, the magnitude and distribution of T_{max} input into the LE model were a required assumption. Fig. 13 illustrates three T_{max} distribution functions (uniform, linear, and trapezoidal) typically assumed in LE analysis. As shown in Fig. 13, the distribution function D_{Tmax} is defined as the ratio of the maximum mobilized load in each reinforcement layer, T_{max}, to the maximum loads of all reinforcement layers, max(T_{max}). The D_{Tmax} value reflects the normalized value of T_{max} as a function of the normalized elevation of $Y = y/H$. Detailed discussions of three tensile load distribution are referred to Leshchinsky et al. [18] and Mohamed et al. [24]. In the current study, the three T_{max} distribution functions were applied in LE analyses to calculate the T_{max} value for each reinforcement layer in a limit state (FS = 1.0).

In the FHWA design guidelines, the reinforcement tensile load at the maximum tension line can be estimated as follows:

$$T_{max} = \left(\frac{k_r}{K_a}\right) K_a \sigma_v S_v \tag{14}$$

where T_{max} is the maximum reinforcement load of each reinforcement layer, k_r/K_a is the normalized lateral earth pressure coefficient

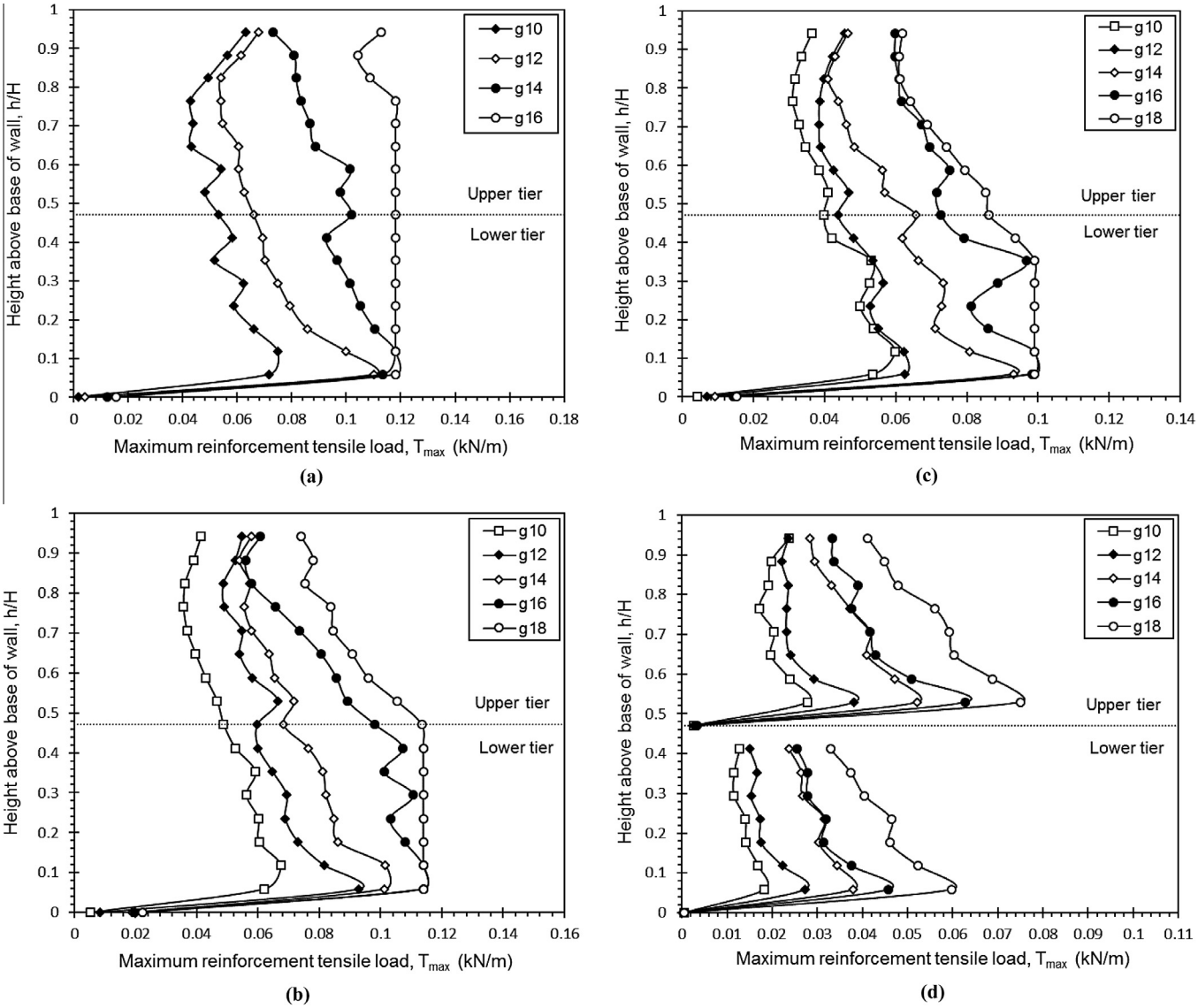

Fig. 12. Development and distribution of maximum reinforcement tensile load with depth for various *g*-level: (a) Test S1; (b) Test C4; (c) Test C6; (d) Test I11.

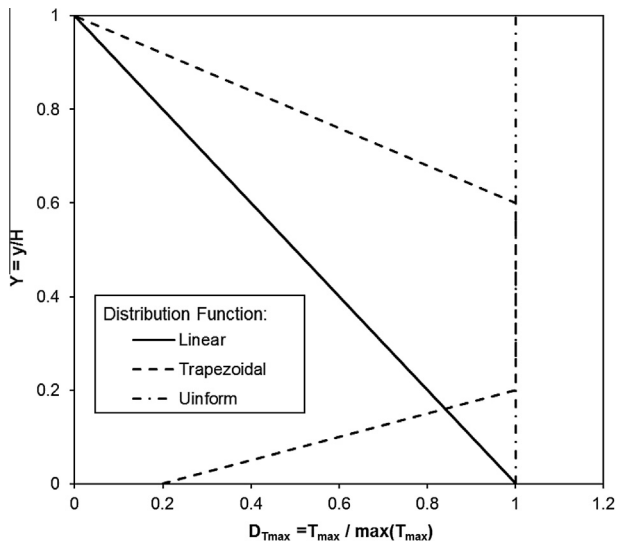

Fig. 13. Three typical reinforcement tensile load distribution functions assumed in the LE analysis (after [18]).

(for GRS walls, the k_r/K_a = 1.0 and remains constant throughout the wall depth), K_a is the active earth pressure coefficient, σ_v is the effective overburden pressure at the maximum tension line, calculated using Eqs. (3)–(8), and S_v is the vertical spacing between reinforcement layers.

Fig. 14 shows the comparison results of the T_{max} distributions with depth at wall failure obtained from FE, LE, and FHWA design guidelines. The magnitude and distribution of T_{max} calculated by assuming uniform distribution in the LE method is more consistent with the FE results compared with those calculated by assuming linear and trapezoidal distributions. The comparison results suggest that the uniform distribution of T_{max} can adequately capture the T_{max} value and its distribution with depth at wall failure; consequently, the uniform distribution of T_{max} is adopted in LE analyses. Fig. 14 also indicates that regardless of using ϕ_{tx} or ϕ_{ps}, the method suggested in the FHWA design guidelines cannot adequately describe the T_{max} distribution at wall failure, resulting in an underestimate of the T_{max} value in the upper part of the upper tier and a significant overestimate of the T_{max} value in the lower tier.

Fig. 15 shows a comparison of the max(T_{max}), the maximum tensile loads of all reinforcement layers, predicted by various

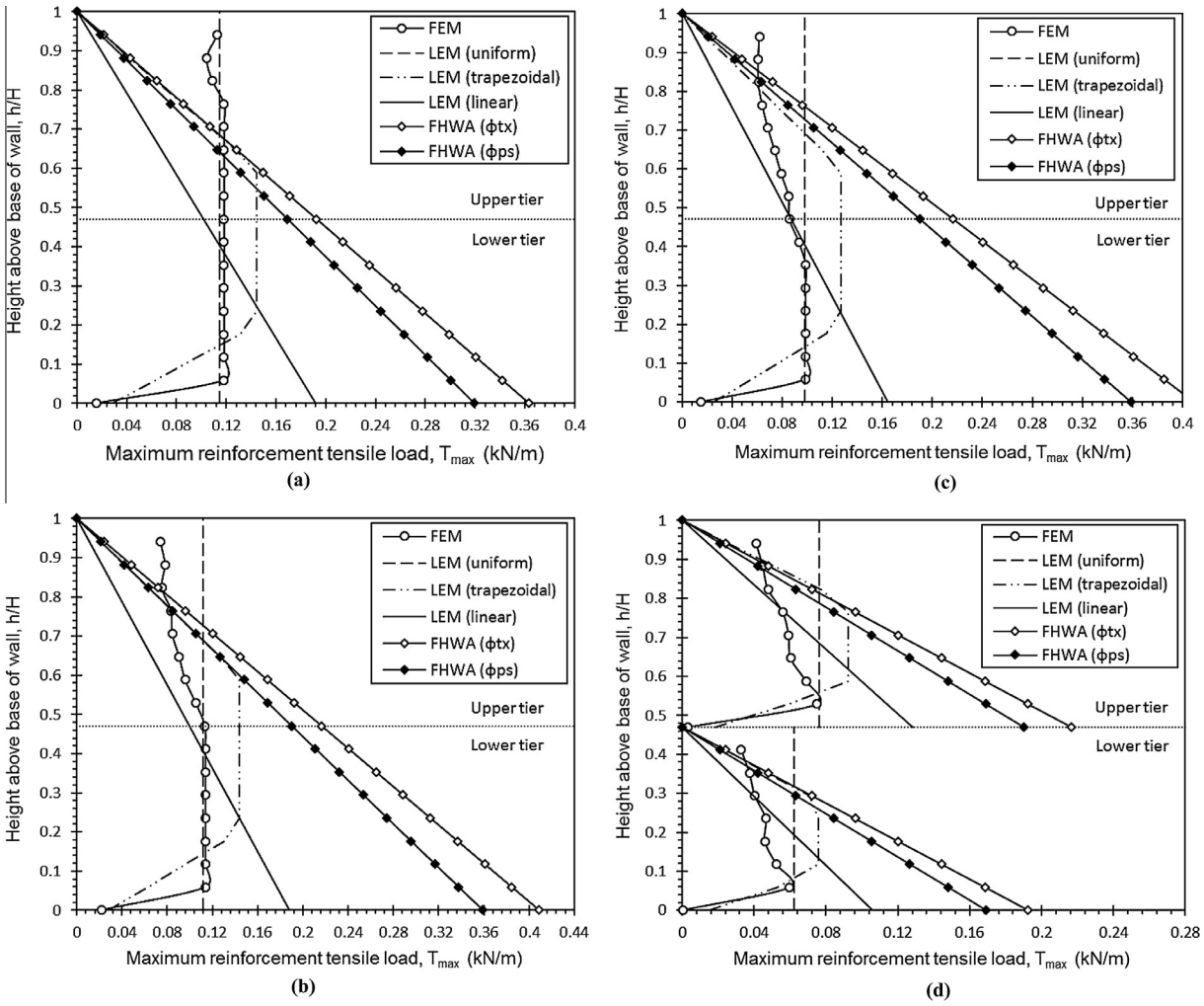

Fig. 14. Comparison of the distributions of the maximum reinforcement tensile load with depth predicted by FEM, LEM and FHWA: (a) Test S1; (b) Test C4; (c) Test C6; (d) Test I11.

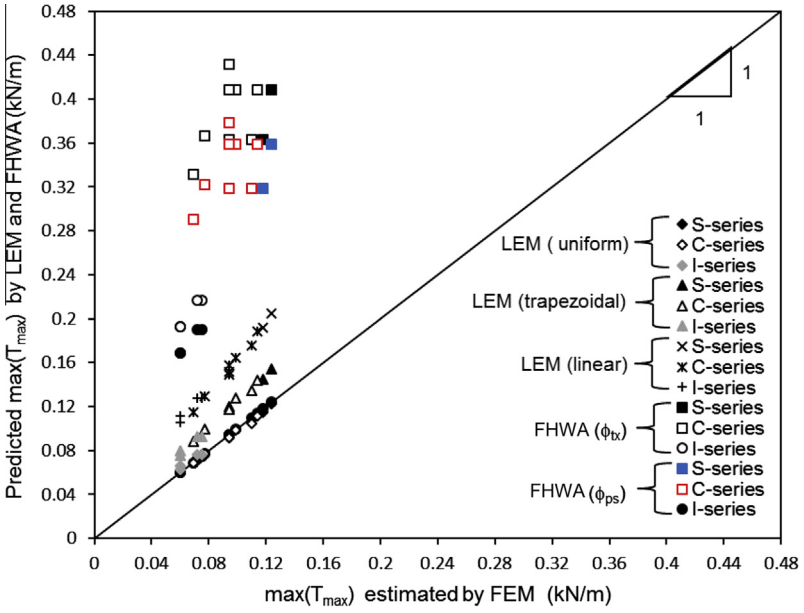

Fig. 15. Comparison of max(T_{max}) predicted by FEM, LEM and FHWA for all centrifuge models.

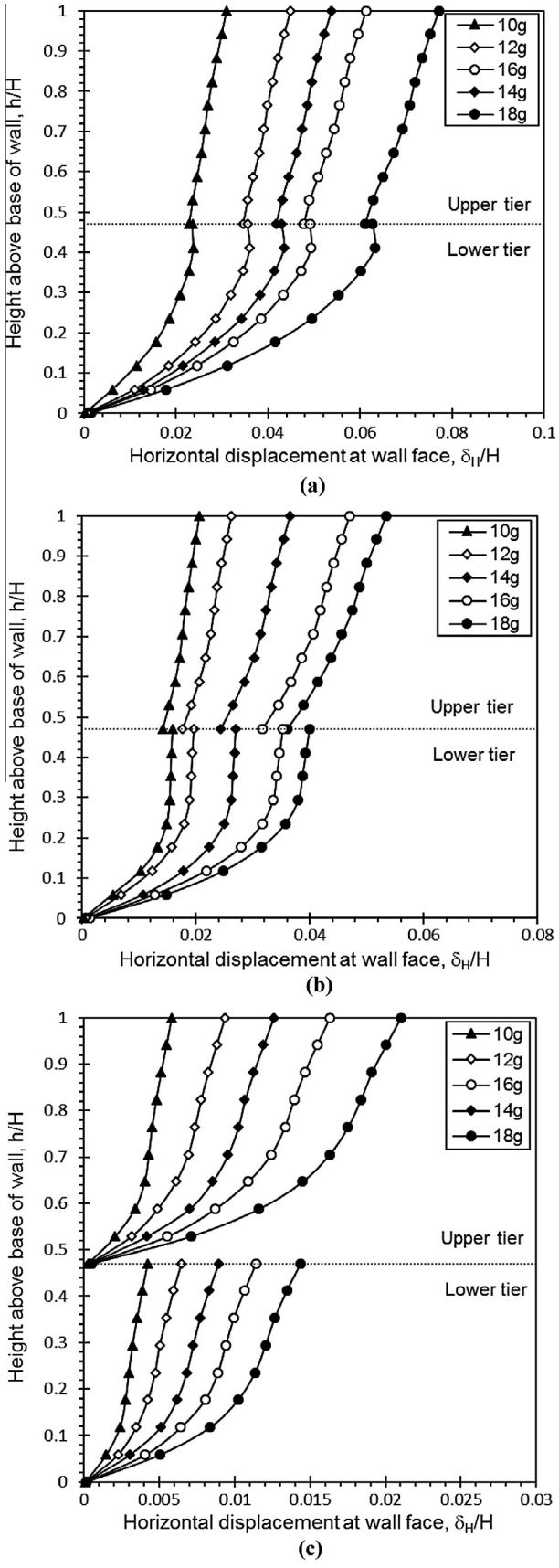

Fig. 16. Development of horizontal deformation at wall face: (a) Test S2; (b) Test C6; (c) Test I11.

methods. The max(T_{max}) value is typically adopted to determine the required long-term strength of reinforcement in the design. Fig. 15 demonstrates that the max(T_{max}) results obtained from FE are in satisfactory agreement with the results obtained from the LE method using the uniform distribution of T_{max}. Table 1 also provides the max(T_{max}) values predicted by FE and LE using the uniform distribution of T_{max}. Table 1 also indicates that only small differences between the sum values of T_{max} for all reinforcement layers (i.e., $\Sigma(T_{max})$) are obtained from FE and LE with uniform distribution, implying that the system requires an equal total amount of resistance from reinforcements to maintain system equilibrium. As shown in Fig. 15, the LE method with linear and trapezoidal distributions and FHWA design guidelines overly predict the max(T_{max}) values. The loads predicted by FHWA were the most conservative, averaging 3–5 times greater than FE estimated values. Yoo and Kim [38] also reported the conservative calculation of reinforced tensile loads by using FHWA. Overall, it can be concluded that using the LE max (T_{max}) value with uniform distribution of T_{max} produces a simple and cost-effective design.

5.3. Horizontal wall deformation

Fig. 16 shows the development and patterns of horizontal wall deformation, δ_H, in Tests S2, C6, and I11. Fig. 16 indicates that a cantilever-type deformation pattern prevails in the facing deformation profiles and the wall deformation increases proportionally with increased g-level. Maximum horizontal wall deformations, $\delta_{H,max}$, were observed at the top of the upper tier. Except for the independent wall, a significant translational movement occurred at the wall base of the upper tier, approximately over 70% of the maximum deformation at the top, primarily because of lateral movements of the lower tier.

Yoo and Kim [38] also reported the cantilever-type wall movement pattern in both the upper and lower tiers of the full-scale wall under surcharge conditions. Stuedlein et al. [33] and Yoo and Jung [37] observed other deformation patterns such as the concave type with maximum deformations occurring near the base or at the mid-height of the two-tier walls. Differences in deformation patterns at the wall face are likely influenced by surcharge,

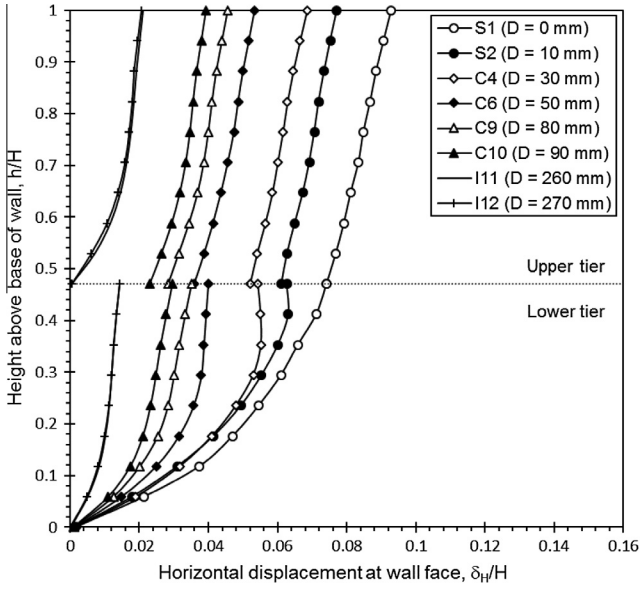

Fig. 17. Effect of offset distance on horizontal wall deformation at wall failure.

foundation, face types, and differential settlement conditions within the reinforced soil zone.

Fig. 17 illustrates the effect of the offset distance on horizontal wall deformation compared at the moment of wall failure. An increase in the offset distance reduces horizontal wall deformation in both the upper and lower tiers. The horizontal wall deformation in a single wall is higher than that in compound and independent walls. When the offset equals or exceeds 260 mm (independent walls), the decrease in horizontal wall deformation becomes negligible. The translational movement occurring at the wall base of the upper tier also decreases with a reduced offset distance and reduces to zero at independent walls. These results suggest that the interaction between the two tiers attenuates when they separate farther apart.

5.4. Effect of the offset distance on two-tier interaction

The two tiers interact through the equivalent surcharge from the upper tier acting on the lower tier and the deformation of the lower tier influencing the behavior of the upper tier. Consequently, the two tiers mutually affect each other and cause additional wall deformation and reinforcement load in both the upper and lower tiers when compared with a wall of the same height as each tier. This is demonstrated using the FE results obtained in the current study.

Fig. 18 shows the effect of the offset distance on the max(T_{max}) and $\delta_{H,max}$ in both the upper and lower tiers at wall failure. The results in Fig. 18a show decreased max(T_{max}) values in both the upper and lower tiers with an increased offset distance, reaching a constant value beyond the critical offset distance D_{cr}. The decreasing trend of the max(T_{max}) values in the lower tier suggests that as the offset distance increases, the influence of the equivalent surcharge from the upper tier on reinforcements in the lower tier decreases. The highest max(T_{max}) value was acquired from single walls because of their small offset distances, which induced high overburden pressure on the reinforcement. Independent walls had the lowest max(T_{max}) values because the large offset distance decreased the overburden pressure from the upper tier acting on reinforcements in the lower tier. The max(T_{max}) values in the upper tiers also show the same decreasing trend, caused by reduced wall deformation at the lower tier with an increased offset distance. The ratio of max(T_{max}) when two tiers have full interaction(i.e., a single

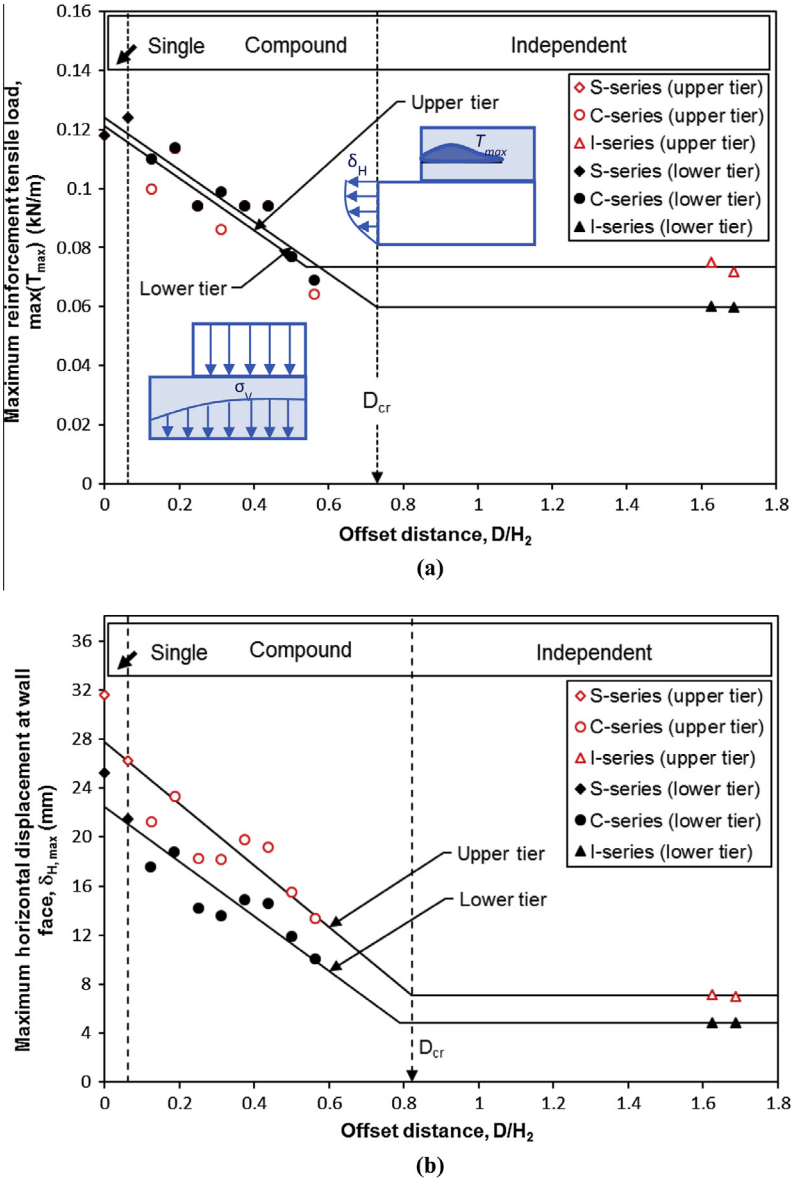

Fig. 18. Effect of offset distance on: (a) maximum reinforcement tensile load; (b) horizontal wall deformation.

Table 4
Comparison of critical offset distances determined by various methods.

Current design approach and previous researches	Critical offset distance, D_{cr}	Method
FHWA [10,5]	$\tan(90^\circ - \phi)H_2$ (=1.21H_2 with $\phi_{tx} = 39.5^o$)	Empirical
NCMA [25]	L_2 for internal analysis, $L_2 + X_2$ for external analysis[a]	Empirical
Leshchinsky and Han [17]	0.80H_2	Limit equilibrium
Yoo et al. [36]	0.80H_2	Finite element
Mohamed et al. [24]	0.70H_2	Limit equilibrium
This study	0.73H_2	Finite element (by max(T_{max}))
	0.82H_2	Finite element (by δ_H)

[a] $X_2 = (H_2 + D/500)\tan\alpha$, where α is the inclination angle of the Coulomb failure surface, for tiered walls with vertical tiers and horizontal offset distances.

wall) to that when no interaction occurs between two tiers (i.e., independent wall) is approximately 1.7 and 2 in the upper and lower tiers, respectively.

Fig. 18b shows a similar trend in the results of $\delta_{H,max}$ in both the upper and lower tiers. The results in Fig. 18b show that the $\delta_{H,max}$ value decreases as the offset distance increases and reaches a constant value beyond the critical offset distance D_{cr}. This observation supports the previous statement that the interaction between the two tiers reduces as the offset distance increases. The ratio of $\delta_{H,max}$ in the single wall to that in the independent wall is approximately 3.5 and 4.5 in the upper and lower tiers, respectively. The FE findings are consistent with previous studies [37,38]. They observed that the interaction between two tiers substantially increased the wall movements and the reinforcement strains in both the upper and lower tiers. The FHWA design guidelines do not fully consider this mutual interaction between two tiers. The FHWA design guidelines considers only the upper tier influence on the lower tier regarding the equivalent surcharge acting on the lower tier, but do not address the lower tier influence on the upper tier regarding the lower tier deformation amplifying the deformation and the subsequent mobilization of reinforcement loads at the upper tier because they suggest designing the upper tier as a single wall.

5.5. Critical offset distance

The critical offset distance D_{cr} shown in Fig. 18 is the offset distance beyond which two tiers act independently. In Fig. 18, $D_{cr} = 0.73H_2$ was identified when the decreased max(T_{max}) value with increased D reached a constant value (the intersection of two trend lines in Fig. 18a), and $D_{cr} = 0.82H_2$ was identified when the decreased δ_H value with increased D reached a constant value. Yoo et al. [36] also assessed the internal stability of two-tier GRS walls using reduced-scale physical models and FE simulations. The critical offset distance was $D_{cr} = 0.8H_2$ using FE simulation when the increase in the factor of safety (FS) with the increase in D reached a constant value. Leshchinsky and Han [17] analyzed multitier walls numerically by comparing the results obtained from FE and LE analyses. The $D_{cr} = 0.8H_2$ was determined using LE analysis when decreased required tensile strength of the reinforcement with increased D reached a constant value.

Table 4 lists the critical offset distance, D_{cr}, values obtained from FE using max(T_{max}), and δ_H results in this study, reported by design guidelines and previous studies. The results in Table 4 indicate that the D_{cr} value obtained in this study and previous studies is only slightly different. In general, the D_{cr} ranges from 0.7–0.8H_2, which is substantially lower than the values recommended in FHWA and NCMA design guidelines. The D_{cr} value recommended by the FHWA is approximately 1.5 times greater than those determined using FE in this study, and reported by previous studies [17,36]. Consequently, using the D_{cr} value provided in the current design guidelines would likely result in a conservative design.

6. Conclusion

This study presents the procedure and results of FE analyses of a series centrifuge tests on two-tier GRS wall models with various offset distances. The FE results were used to investigate the mobilization and distribution of reinforcement tensile loads, effective overburden pressure, and the horizontal wall deformation of two-tier walls with various offset distances. Based on the details of the FE findings on the interaction between two tiers and design implications for multitier GRS walls, the conclusions of this study are summarized as follows:

- Excellent agreement was obtained among the centrifuge models, FE, and LE with a noncircular failure surface in locating failure surface. The maximum tension lines in FHWA design guidelines depict failure surfaces at a long distance from the wall face, particularly for the upper part of the upper tier, resulting in an overestimation of the required reinforcement lengths and, consequently, a conservative design against pullout.
- The FE results demonstrated that the modified Gray's elastic solution is more realistic in calculating the effective overburden pressure on the lower tier with increased offset distance, compared with the FHWA design guideline approach.
- The FE findings showed a nearly uniform distribution of maximum reinforcement tensile loads with depth at wall failure, confirming the assumed uniform distribution of reinforced tensile loads used in the LE analysis as reasonable.
- The calculated max(T_{max}) values obtained from FE analyses agreed with the results obtained from the LE method with uniform distribution. However, over predictions of max(T_{max}) values were obtained using FHWA and the LE method with linear and trapezoidal distributions.
- An increased offset distance decreases the max(T_{max}) and δ_H values predicted by FE in both the upper and lower ties, demonstrating that the two tiers mutually affect each other and can cause additional wall deformation and reinforcement strain in both the upper and lower tiers. However, the FHWA design guidelines only considers the influence of the upper tier as the equivalent surcharge on the lower tier but do not address the influence of the lower tier on the upper tier.
- The critical offset distances $D_{cr} = 0.73H_2$ by max(T_{max}) and $D_{cr} = 0.8\ H_2$ by δ_H identified in this study agree with the D_{cr} values reported in previous studies, and are considerably lower than the values recommended in FHWA and NCMA design guidelines.

Finally, this study addressed only the results of FE analyses for centrifuge modeling of two-tier GRS walls with various offset distances. Issues related to field conditions, such as extra deformation and reinforcement loads induced by compaction, soft foundation, and GRS walls with more than two tiers, require further investigation.

Acknowledgments

This research work was sponsored by the Taiwan National Science Council. The financial support for the third author during his Ph.D. study was provided by the Taiwan Ministry of Education under the Grant for "Aim for the Top-Tier University Project". These financial supports are gratefully acknowledged. The authors also sincerely appreciate the constructive comments by the anonymous reviewers.

References

[1] Allen TM, Bathurst RJ. Soil reinforcement loads in geosynthetic walls at working stress conditions. Geosynth Int 2002;9(5–6):525–66.
[2] Allen TM, Bathurst RJ, Holtz RD, Walters D, Lee WF. A new working stress method for prediction of reinforcement loads in geosynthetic walls. Can Geotech J 2003;40(5):976–94.
[3] ASTM D4595. Standard test method for tensile properties of geotextiles by the wide-width strip method. In: Annual book of ASTM standards, vol. 4.09, West Conshohocken, PA; 1996. p. 698–708.
[4] Bathurst RJ, Miyata Y, Nernheim A, Allen TM. Refinement of K-stiffness method for geosynthetic reinforced soil walls. Geosynth Int 2008;15(4):269–95.
[5] Berg R, Christopher BR, Samtani N. Design of mechanically stabilized earth walls and reinforced soil slopes, vols. I and II. Report no. FHWA-NHI-10-024. Federal Highway Administration; 2009. 684 pp.
[6] Bolton MD. The strength and dilatancy of sands. Geotechnique 1986;36(1):65–78.
[7] Boyle SR, Gallagher M, Holtz RD. Influence of strain rate, specimen length and confinement in measured geotextile properties. Geosynth Int 1996;3(2):205–25.
[8] Christopher BR, Holtz RD, Bell WD. New tests for determining the in-soil stress–strain properties of geotextiles. In: Proceedings of the third international conference on geotextile, Vienna, Austria; 1986. p. 683–6.
[9] Christopher BR, Leshchinsky D, Stulgis R. Geosynthetic-reinforced soil walls and slopes: US perspective. International perspectives on soil reinforcement applications. ASCE geotechnical special publication no. 141. Reston, Virginia: ASCE Press; January 2005. 166 p. ISBN: 0-7844-0769-X.
[10] Elias V, Christopher BR, Berg R. Mechanically stabilized earth walls and reinforced soil slopes design and construction guidelines. Report no. FHWA-NHI-00-043. Washington, DC, USA: National Highway Institute, Federal Highway Administration; 2001. 418 pp.
[11] Gray H. Stress distribution in elastic solids. In: Proceedings of second international conference on soil mechanics and foundation engineering, Cambridge; 1936. p. 157–68.
[12] Hatami K, Bathurst RJ. Development and verification of t numerical model for the analysis of geosynthetic-reinforced soil segmental walls under working stress conditions. Can Geotech J 2005;67(4):1066–85.
[13] Hatami K, Bathurst RJ. Numerical model for reinforced soil segmental walls under surcharge loading. J Geotech Geoenviron Eng ASCE 2006;132(6):673–84.
[14] Hung WY. Breaking failure behavior and internal stability analysis of geosynthetic reinforced earth walls. PhD dissertation. National Central University, Jhongli, Taiwan; 2008. 200 pp.
[15] Karpurapu RG, Bathurst RJ. Behaviour of geosynthetic reinforced soil retaining walls using the finite element method. Comput Geotech 1995;17(3):279–99.
[16] Lade PV, Lee KL. Engineering properties of soils. Report UCLA-ENG-7652. Los Angeles, CA: University of California; 1976. 145 pp.
[17] Leshchinsky D, Han J. Geosynthetic reinforced multi-tiered walls. J Geotech Geoenviron Eng ASCE 2004;130(12):1225–35.
[18] Leshchinsky D, Zhu F, Meehan C. Required unfactored strength of geosynthetic in reinforced earth structures. J Geotech Geoenviron Eng ASCE 2010;136(2):281–9.
[19] Ling HI, Cardany CP, Sun L-X, Hashimoto H. Finite element analysis of a geosynthetic-reinforced soil retaining wall with concrete-block facing. Geosynth Int 2000;7(3):163–88.
[20] Liu C-N, Yang K-H, Ho Y-H, Chang C-M. Lessons learned from three failures on a high steep geogrid-reinforced slope. Geotext Geomembr 2012;34:131–43.
[21] Liu H. Comparing the seismic responses of single- and multi-tiered geosynthetic reinforced soil walls. Geo-Frontiers 2011;2011:3478–86.
[22] Lopes ML, Cardoso AS, Yeo KC. Modelling performance of a sloped reinforced soil wall using creep function. Geotext Geomembr 1994;13(3):181–97.
[23] Marachi N, Duncan JM, Chan C, Seed HB. In: Yong RN, Townsend FC, editors. Plane-strain testing of sand. Laboratory shear strength of soil. ASTM special technical bulletin 740. West Conshohocken: American Society for Testing and Materials; 1981. p. 294–302.
[24] Mohamed SBA, Yang K-H, Hung WY. Limit equilibrium analyses of geosynthetic-reinforced two-tiered walls: calibration from centrifuge tests. Geotext Geomembr 2013;41:1–16.
[25] NCMA. Design manual for segmental retaining walls. 3rd ed. Herndon, Virginia, USA: National Concrete Masonry Association; 2010. 282 pp.
[26] Osborne WN, Wright SG. An examination of design procedures for single- and multi-tier mechanically stabilized earth walls. Report no. FHWA/TX-05/0-4485-1, Austin, Texas; 2004. 202 pp.
[27] PLAXIS. Plaxis finite element code for soil and rock analyses, version 8.2, P.O. Box 572, 2600 AN Delft, Netherlands; 2005.
[28] Porbaha A, Goodings DJ. Centrifuge modeling of geotextile reinforced cohesive soil retaining walls. J Geotech Eng ASCE 1996;122(10):840–8.
[29] Rocscience. Slide Ver. 6.009-2D limit equilibrium slope stability analysis. Toronto, Canada: Rocscience, Inc.; 2011.
[30] Schanz T, Vermeer PA, Bonnier PG. The Hardening Soil model: formulation and verification. In: Proc beyond 2000 in computational geotechnics, Balkema, Rotterdam, Netherlands; 1999. p. 281–90.
[31] Spencer E. A method of analysis of the stability of embankments assuming parallel inter-slice forces. Geotechnique 1967;24(4):661–5.
[32] Stuedlein AW, Allen TM, Holtz RD, Christopher BR. Assessment of reinforcement strains in very tall mechanically stabilized earth walls. J Geotech Geoenviron Eng 2012;138(3):345–56.
[33] Stuedlein AW, Bailey M, Lindquist D, Sankey J, Neely WJ. Design and performance of a 46-m-high MSE wall. J Geotech Geoenviron Eng 2010;136(6):786–96.
[34] Wright SG. Design guidelines for multi-tiered MSE walls. Report no. FHWA/TX-05/0-4485-2, Austin, Texas; 2005. 118 pp.
[35] Yang K-H, Zornberg JG, Liu C-N, Lin H-D. Stress distribution and development within geosynthetic-reinforced soil slope. Geosynth Int 2012;19(1):62–78.
[36] Yoo C, Jang YS, Park IJ. Internal stability of geosynthetic-reinforced soil walls in tiered configuration. Geosynth Int 2011;18(2):74–83.
[37] Yoo C, Jung HS. Measured behavior of a geosynthetic reinforced segmental retaining wall in a tiered configuration. Geotext Geomembr 2004;22(5):359–76.
[38] Yoo C, Kim SB. Performance of a two-tier geosynthetic reinforced segmental retaining wall under a surcharge load: full-scale load test and 3D finite element analysis. Geotext Geomembr 2008;26(6):447–518.
[39] Yoo C, Song AR. Effect of foundation yielding on performance of two-tier geosynthetic reinforced segmental retaining walls: a numerical investigation. Geosynth Int 2007;20(3):110–20.
[40] Zornberg JG. Performance of geotextile reinforced soil structures. PhD dissertation. Department of Civil Engineering, University of California, Berkeley, CA, USA; 1994. 504 pp.
[41] Zornberg JG, Sitar N, Mitchell JK. Performance of geosynthetic reinforced slopes at failure. J Geotech Geoenviron Eng ASCE 1998;124(8):670–83.
[42] Zornberg JG, Sitar N, Mitchell JK. Limit equilibrium as basis for design of geosynthetic reinforced slopes. J Geotech Geoenviron Eng ASCE 1998;124(8):684–98.